Chemical Engineering Journal 449 (2022) 137784

Contents lists available at ScienceDirect

Chemical Engineering Journal

journal homepage: www.elsevier.com/locate/cej

Effective elimination of tetracycline antibiotics via photoactivated SR-AOP over vivianite: A new application approach of phosphorus recovery product from WWTP

Xiao-Hong Yi [a,b], Tian-Yu Wang [a,b], Hong-Yu Chu [a,b], Ya Gao [a,b], Chong-Chen Wang [a,b,*], Yu-Jia Li [a,b], Long Chen [c], Peng Wang [a,b,*], Huifen Fu [a,b], Chen Zhao [a,b], Wen Liu [c]

[a] Beijing Key Laboratory of Functional Materials for Building Structure and Environment Remediation, School of Environment and Energy Engineering, Beijing University of Civil Engineering and Architecture, Beijing 100044, China
[b] Beijing Energy Conservation & Sustainable Urban and Rural Development Provincial and Ministry Co-construction Collaboration Innovation Center, Beijing University of Civil Engineering and Architecture, Beijing 100044, China
[c] College of Environmental Sciences and Engineering, Peking University, The Key Laboratory of Water and Sediment Sciences, Ministry of Education, Beijing 100871, China

ARTICLE INFO

Keywords:
Vivianite
Photoactivation
Peroxydisulfate
Tetracycline antibiotics
Degradation

ABSTRACT

$Fe_3(PO_4)_2{\cdot}8H_2O$ (Vivianite) is one of the potential phosphorus recovery products from wastewater treatment plant (WWTP). In this study, we first discovered that vivianite can effectively photoactivate peroxodisulfate (PDS) to produce some reactive oxygen species (ROS) for tetracycline antibiotics (TCs) degradation. The results demonstrated that vivianite could efficiently activate PDS to achieve 100% removal of TCs under LED UV light (UVL), visible light (VL) or real solar light (SL) irradiation within 10 min, respectively. More importantly, ca. 80%, 78% and 40%~58% of TOC removal efficiencies were achieved under UVL, VL and SL irradiation within 30 min, respectively. As well, toxicological simulation and antibacterial studies showed that the aquatic toxicity of the TCs intermediates was lower than those of the original TCs. This work provided new insights into the application of photoactivated sulfate radical-advanced oxidation process (SR-AOP) for organic pollutants degradation over vivianite, which may encourage the recovery and utilization of vivianite in the wastewater treatment process.

1. Introduction

It was essential to achieve phosphorus recovery from wastewater due to both the global shortage and the wide eutrophication [1–3]. From the view of 3Rs (reduce, recycle and reuse) approach, wastewater should be recognized as valuable resource from which the phosphorus can be recovered to yield high added valuable products. Among the different recovery products of phosphorous in the wastewater treatment plant, $Fe_3(PO_4)_2{\cdot}8H_2O$ (vivianite) produced in the anaerobic section attracted increasing attentions considering high added economic value [4,5]. Besides as plant fertilizer, vivianite was adopted as functional material to eliminate different heavy metals like Cu(II) [6], Zn(II) [7], As(V) [8,9], U(V) [10], Cr(VI) [11], Pb(II) [12], Hg [13], Se(IV) and Cd(II) [14]. It was observed that the Fe(II) in the vivianite might be partially oxidated into Fe(III) [15–17], in which the co-existing Fe(II) and Fe(III) might achieve Fe(II)/Fe(III) transformation to activate the sulfate radical-advanced oxidation process (SR-AOP).

It was well known that increasing Fe-based heterogenous catalysts were introduced to activate peroxodisulfate (PDS) and peroxymonosulfate (PMS) for accomplishing advanced oxidation processes (AOPs) to degrade different organic pollutants [18–20] due to the abundant iron elements in earth crust minerals and low cost in addition to their non-toxic nature [21–24]. Our previous works reported the photoactivated or photocatalysis-activated persulfate (PS) by MIL-88A (Fe)/cotton fibers [25], PDINH/MIL-88A(Fe) [26] and Fe_3O_4 catalyst derived from MIL-88A(Fe) [27] for organic pollutants degradation. The boosted AOP degradation performances were ascribed to the synergistic effects of direct PS photoactivation, direct electron transfer activation of

* Corresponding authors at: Beijing Key Laboratory of Functional Materials for Building Structure and Environment Remediation, School of Environment and Energy Engineering, Beijing University of Civil Engineering and Architecture, Beijing 100044, China.
E-mail addresses: wangchongchen@bucea.edu.cn (C.-C. Wang), wangpeng@bucea.edu.cn (P. Wang).

https://doi.org/10.1016/j.cej.2022.137784
Received 10 May 2022; Received in revised form 15 June 2022; Accepted 23 June 2022
Available online 25 June 2022

PS over the catalyst and indirect electron transfer PS activation resulted from Fe(II)/Fe(III) transformation.

Tetracycline antibiotics (TCs), including tetracycline (TTC), oxytetracycline (OTC), and chlortetracycline (CTC), are widely used for bacterial infections treatment toward humans and animals due to their low cost and great therapeutic values [28]. For example, TCs are the top antimicrobial drugs consumed in the U.S. and the European Union [29], in which the majority of the parent compounds up to 75% is discharged into the environment with urine owing to the poor degradability in human or animal bodies [30]. Tetracyclines have been detected in different water bodies such as surface water, groundwater and even drinking water, which exerted serious threat to ecosystems and human health even at low or trace levels [31]. The presence of tetracyclines in the surrounding environment has become a growing concern, and the treatment of its wastewater has become a pressing issue today [32].

Considering the potential transformation of Fe(II)/Fe(III), the vivianite was adopted the photoactivated SR-AOP catalysts to stimulate PDS for degrading different TCs like TTC, OTC and CTC upon the irradiation of UV light, visible light and solar light, respectively. The influence of various experimental parameters like initial TCs concentrations, the PDS dosage, initial solution pH, and the co-existing ions toward the SR-AOP performances were explored. The toxicity of the TCs and their intermediates was assessed by both the Toxicity Estimation Software (T.E.S.T.) and antibacterial tests. The goal of this research is to affirm the possibility of vivianite as SR-AOP catalyst for effective elimination toward different tetracycline antibiotics, which will provide a brand-new strategy for the utilization of recovered products from the wastewater treatment plant.

2. Materials and methods

2.1. The chemicals reagents, instruments, characterization and analytical methods

The chemicals reagents, instruments, characterizations and analytical methods are provided in the Supplementary Materials. $Fe_3(PO_4)_2{\cdot}8H_2O$ (Vivianite, 98%) was purchased from ShangHai EKEAR Bio&Tech Co., Ltd.

2.2. The photoactivated SR-AOP experiment

20.0 mg vivianite and 50.0 mL TTC, OTC or CTC aqueous solution (10.0 mg/L) was put in cylinder type quartz glass photoreactor (PCX50B or PCX50C, Beijing Perfectlight Technology Co., Ltd.), which was stirred for 1 h in dark to achieve adsorption–desorption equilibrium [26,33]. Specifically, the stirring speed of the reactor was 200 r/min. Subsequently, a certain amount of PDS was added to initiate degradation reaction upon the irradiation of 300 ± 50 mW LED UV light (PCX50B), 300 ± 50 mW LED visible light (PCX50C) or real solar light (Daxing campus of BUCEA, 39°44′45″ N, 116°16′37″ E, 32 °C, August 7th, 2021) (**Fig. S1**). Both the LED UV light and LED visible light are emitted from the bottom of the quartz glass photoreactor. During the illumination period, 1.0 mL of the supernatant was collected every 1 min or 2 min to determine the residual concentration of TCs, immediately quenched with 10 μL of methanol and further filtered through a 0.22 μm Millipore film [26]. The residual concentration for TCs was analyzed by UHPLC (Thermo Scientific Vanquish Flex) equipped with a C18 reversed-phase column (2.1 mm × 100 mm, 1.7 μm) and a UV–Vis detector. The analytical methods were described detailly in Text S3.

3. Results and discussion

3.1. Characterizations

The surface morphology observed (Fig. 1**a and 1b**) that the commercially available vivianite demonstrated the multilayered flower-like configuration stacked from the 2D thin sheets (length, 3–15 μm; width, 1–10 μm; thickness, 200–800 nm), which was comparable to the previously reported synthetic vivianite [34,35]. In addition, the EDS determination (Fig. 1**c**) showed that the target elements (Fe, P and O) were uniformly distributed over vivianite, the Fe/P ratio of vivianite crystals was close to 1.5, which matched perfectly with the stoichiometric formula of vivianite [35,36].

It was found that the PXRD patterns (Fig. 2**a**) of commercial vivianite were in good agreement with the standard PXRD patterns of vivianite (PDF#01–084-0341). Specifically, the characteristic peaks of vivianite at 2θ of 10.3°, 13.1° and 18.2° were ascribed to the diffraction planes of (0 1 0), (−1 1 0) and (1 1 0), respectively. As illustrated in **Fig. S2**, the absorption bands at 3415 and 1630 cm^{-1} can be ascribed to the stretching and bending vibrations of O–H group of lattice water molecules [37,38]. The particles show strong transmission bands at 1030 and 547 cm^{-1} matched well with the vibration of P–O in iron phosphates [38,39]. The surface area determination showed that the commercial vivianite displayed a specific surface area (SSA) of 6.7 (m^2/g), with mesoporous structure of average pore size being 13.5 nm (**Fig. S3**).

The optical activity and light absorption ability of vivianite were assessed by UV–vis DRS spectroscopy. It was noteworthy that vivianite exhibited strong absorption response in the ultraviolet and visible

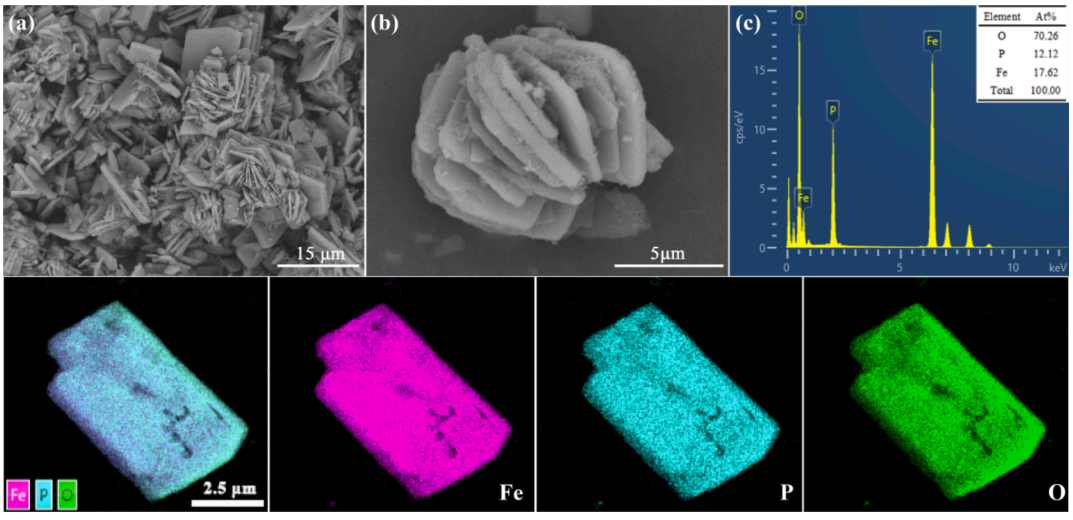

Fig. 1. (a-b) FESEM images of vivianite; (c) corresponding EDS patterns of vivianite.

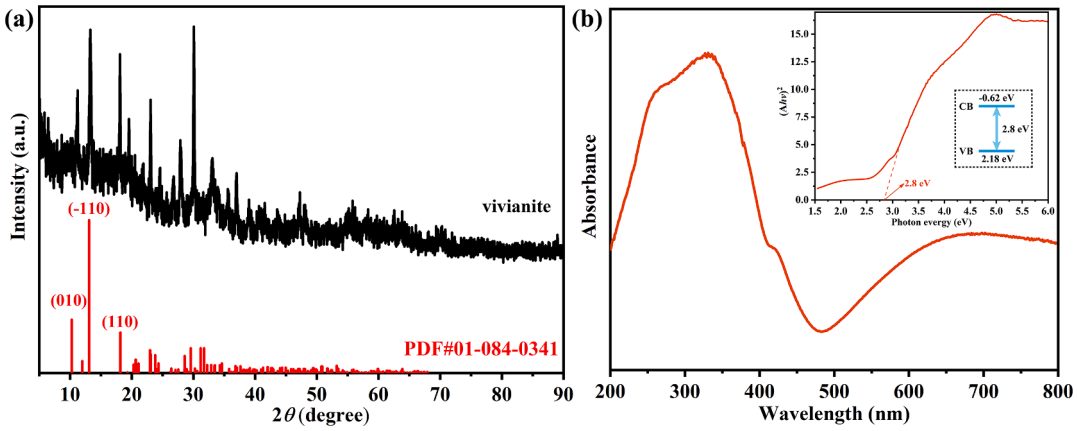

Fig. 2. (a) The PXRD patterns and (b) The UV–vis DRS spectra (inset: the E_g plots) of vivianite.

region, implying that it can be excited by both UV light and visible light (Fig. 2**b**). The band gap of vivianite was calculated as 2.8 eV (Fig. 2**b insert**). The positive slope of vivianite's linear C^{-2} potential curve (**Fig. S4**) implied that vivianite exhibited the characteristics of *n*-type semiconductor [33,40]. The flat band potential (E_{FB}) of vivianite was found to be −0.31 eV *vs.* Ag/AgCl. As a result, the E_{FB} of vivianite was calculated to be −0.11 eV *vs.* NHE. The position of E_{CB} of n-type semiconductors is ca. 0.1 eV lower than that of E_{FB} [41]. In addition, taking into account the influence of pH, the equation of $E = E_0 - 0.05915 \times pH$ was adopted to adjust the E_{CB} of vivianite [41]. Therefore, the E_{CB} of vivianite was −0.62 eV *vs.* NHE at pH = 7.0. Considering the band gap of 2.8 eV for vivianite and the equation of $E_g = E_{VB} - E_{CB}$, the potential of the E_{VB} of vivianite was 2.18 eV *vs.* NHE.

3.2. The photoactivated SR-AOP of vivianite performances

3.2.1. Tetracycline antibiotics degradation

Tetracycline antibiotics (TCs) were selected as model pollutants with concentration of 10.0 mg/L at initial pH 4.48 to test the photoactivated SR-AOP activities of vivianite. Only ca. 10.4%, 9.6% and 3.8% photolysis of TTC, OTC and CTC can be observed under UV light irradiation without the catalysts (UVL in Fig. 3). The presence of 0.4 g/L vivianite (Vivianite/dark in Fig. 3) in the tetracycline antibiotics solution yielded removal efficiency of 20–25%, indicating its relatively weak adsorption ability toward organics. Under the UV light illumination (Vivianite/UVL in Fig. 3), vivianite exhibited moderate photocatalytic activity, removing about 27.8%, 35.2% and 46.4% of TTC, OTC and CTC within 10 min, respectively, which were mainly ascribed to the production of reactive charge carriers from the UV-light-illuminated vivianite. It can be observed that the addition of PDS to the reaction system can significantly enhance the performance of degrading TTC/OTC/CTC. When PDS was present, approximately 47.1%, 54.6% and 54.8% of TTC, OTC and CTC were removed within 10 min in dark, demonstrating that PDS can directly degrade TCs (PDS/dark). The degradation efficiencies of PDS/UVL system toward TTC, OTC and CTC increased to 65.6%, 65.2% and 86.2%, compared to that of 47.1%, 54.6% and 54.8% for PDS/dark system, reflecting that the PDS could also be activated to produce $^{\bullet}SO_4^-$ via UV light irradiation. Furthermore, vivianite began to exhibit excellent performance in eliminating TTC/OTC/CTC after adding PDS under UV light irradiation (Vivianite/PDS/UVL), and almost all of the TTC/OTC/CTC could be completely degraded within 10 min. These findings indicated that vivianite displayed great catalytic capabilities toward the PDS activation to yield various active species responsible to the decomposition of the tetracycline antibiotics into smaller molecules even ultimate mineralization to H_2O and CO_2.

The pseudo first-order kinetics model ($\ln(C_0/C_t) = -k_{obs}t$) could be

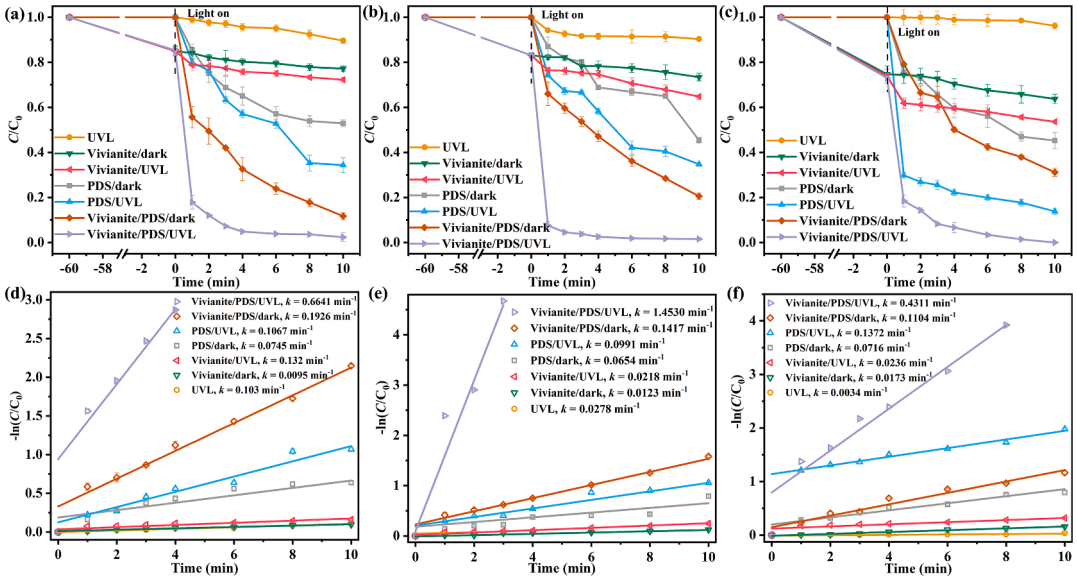

Fig. 3. The tetracycline antibiotics degradation efficiencies (a: TTC, b: OTC and c: CTC) and rates (d: TTC, e: OTC and f: CTC) in different systems. Conditions: catalyst = 0.4 g/L, $[TTC, OTC, CTC]_0$ = 10.0 mg/L, solution volume = 50.0 mL, $[PDS]_0$ = 1.0 mM, unadjusted pH = 4.48.

used to describe the above-stated processes [42], where C_0 and C_t are the initial concentration of TCs and the residual concentration of TCs at any time. As illustrated in Fig. 3**d – 3f**, the value of k_{obs} in vivianite/PDS/UVL system was higher than the other systems. As clearly displayed, the vivianite exhibited excellent activation capacities and PDS utilization efficiencies. The improved performance due to the coupling of vivianite, UV light and PDS processes over sole processes was determined according to the synergy index (SI) with the following expression in Eq. (1) [43–45].

$$\text{Synergy index} = R_{\text{Cata-PDS-UVL}} / (R_{\text{Cata-UVL}} + R_{\text{PDS-UVL}} + R_{\text{Cata-PDS}}) \quad (1)$$

where, $R_{\text{Cata-PDS-UVL}}$, $R_{\text{Cata-UVL}}$, $R_{\text{PDS-UVL}}$ and $R_{\text{Cata-PDS}}$ are the k_{obs} of Vivianite/PDS/UVL, Vivianite/UVL, PDS/UVL and Vivianite/PDS, respectively. The SI values were calculated to be 1.54, 5.53 and 1.59 (>1) for TTC, OTC and CTC, indicating that the combination of vivianite, UVL and PDS system led to a prominent synergetic effect. The results indicated that vivianite seem to be efficient PDS activator for boosted degradation performances toward tetracycline antibiotics in the aquatic samples as being exposed to UV light irradiation.

3.2.1.1. Effect of PDS dosage. The oxidation process is recognized to be influenced by PDS concentration since it is directly related to the production efficiency of the radicals like $^{\bullet}SO_4^-$, $^{\bullet}OH$, and $^{\bullet}O_2^-$ along with the nonradical $^1O_2$. Fig. 4**a – 4c** demonstrated the effect of PDS concentrations on TCs degradation efficiencies. It clearly showed that the degradation efficiencies also can be increased with an increasing of PDS concentration. The improvement of AOP activity can be ascribed to the boosted interaction between vivianite and PDS with increasing PDS dosage, which was inclined to degrade TTC/OTC/CTC through radical and nonradical pathways [46]. However, when PDS dosage was increased to 4.0 mM and 8.0 mM, the degradation efficiency did not increase significantly (as to TTC, the degradation efficiency even decreased slightly). The TCs removal efficiencies maintained stably even PDS dosage was increased to 8.0 mM owing to the occurrence of scavenging reactions like Eqs. (2) and (3) [26,47]. Ultimately, 2.0 mM PDS was selected, considering the economy and efficiency.

$$^{\bullet}SO_4^- + S_2O_8^{2-} \rightarrow {}^{\bullet}S_2O_8^- + {}^{\bullet}OH + SO_4^{2-} \quad (2)$$

$$2\,{}^{\bullet}SO_4^- \rightarrow S_2O_8^{2-} \quad (3)$$

3.2.1.2. Effect of initial pH and concentration of the solution. The solution pH is known to be one of the most important influence parameters on both the catalytic activity and the stability of the catalyst. The tetracycline antibiotics, as amphoteric compounds, possesses three acid-base dissociation constants (pKa): pKa_1 of 3.2–3.57 for tricarbonyl, pKa_2 of 7.3–7.7 for phenolic β-diketone, and pKa_3 of 9.1–9.7 for dimethylamine [48,49]. And the previous studies have shown that autolysis might occur to TCs due to the instability of their ionic structure under alkaline conditions [50]. Therefore, we investigated the degradation performance of vivianite toward TTC at pH ranging from 1.0 to 9.0 (Fig. 4**d**). It was observed that the increasing pH from 1.0 to 3.0 led to the increasing rate constants. However, further pH increasing from 3.0 to 9.0 led to decreasing degradation efficiency. Satisfactorily, ca. 98% TTC removed within 10 min when initial pH = 1.00, 3.00, 4.48, 5.00, 7.00 and 9.00. Zhang et al. reported that the TTC degradation efficiencies decreased from 100% at pH 3.0 to 50% at pH 9.0 [46]. Guan et al. declared that in the $Ni_xFe_{3-x}O_4$/PS system, the TTC degradation efficiency decreased from 86% to ca. 50% when pH increased from 7.0 to 9.0 [51]. In comparison, in this study, the vivianite displayed wider pH suitability, in which it was not required to adjust pH in the subsequent experiments.

Furthermore, the degradation of TTC/OTC/CTC at a low concentration of 1.0 mg/L was also investigated in vivianite/PDS/UVL system. The TTC/OTC/CTC degradation efficiency in vivianite/PDS/UVL system were 100% within 8 min (Fig. 4**e**), further indicating that the vivianite exhibited the excellent catalytic performance on TTC/OTC/CTC degradation.

3.2.2. Tetracycline antibiotics matrix degradation

TTC, OTC and CTC usually co-exist in livestock and aquaculture wastewater at the same time. Therefore, the photoactivated SR-AOP degradation activities of vivianite towards different tetracycline antibiotics matrix (TTC, OTC and CTC) were tested upon the irradiation of UV-LED light. As depicted in Fig. 4**f**, the TTC in the matrix (TCs-TTC) could be removed completely within 6 min upon the irradiation of UV-LED light, and even OTC and CTC in the matrix (TCs-OTC and TCs-CTC) could be removed completely within 1 min, further indicating that the vivianite exhibited the excellent catalytic degradation performance on tetracycline antibiotics. An overview of works published on Fe-based catalysts on TCs degradation by SR-AOP were listed in **Table S1**, in which vivianite exhibited superior SR-AOP activity to its counterpart catalysts.

3.2.2.1. Effect of co-existing inorganic anions and different simulated wastewater. Some inorganic cations found in aquatic environment (such as K^+, Na^+, Ca^{2+} and Mg^{2+}) were assumed to be unable to consume e^- or h^+ due to their stable and maximum oxidation states, which are believed to exert no evident influence on TCs degradation [47,52]. To investigate the practical applications of vivianite/TCs/PDS/UVL system, the different co-existing inorganic ions like Cl^-, NO_3^-, SO_4^- and HCO_3^- with concentrations of 135.30, 13.60, 124.00 and 272.00 mg/L were added

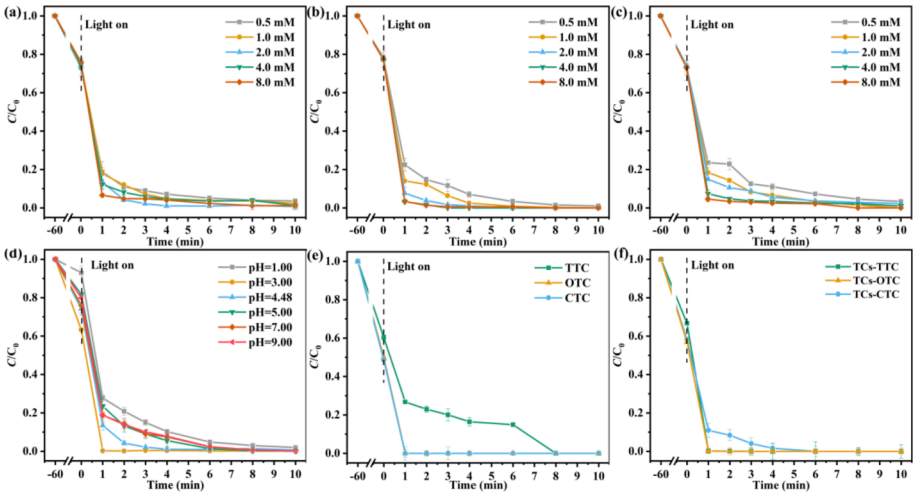

Fig. 4. Effect of PDS dosage in the vivianite/PDS/UVL system: (a) TTC, (b) OTC, (c) CTC. (d) Photoactivated SR-AOP curves for TTC over vivianite under different solution pH conditions. Reaction conditions: catalyst = 0.4 g/L, $[TTC, OTC, CTC]_0$ = 10.0 mg/L, solution volume = 50.0 mL, $[PDS]_0$ = 2.0 mM. (e) Photoactivated SR-AOP curves over vivianite at TTC/OTC/CTC concentration of 1.0 mg/L. Reaction conditions: catalyst = 0.4 g/L, $[TTC, OTC, CTC]_0$ = 1.0 mg/L, solution volume = 50.0 mL, $[PDS]_0$ = 0.2 mM, unadjusted pH = 4.48. (f) Tetracycline antibiotics matrix degradation over vivianite under LED UV light irradiation. Reaction conditions: catalyst = 0.4 g/L, $[TCs\text{-}TTC, TCs\text{-}OTC, TCs\text{-}CTC]_0$ = 3.0 mg/L, solution volume = 50.0 mL, $[PDS]_0$ = 2.0 mM, unadjusted pH = 4.48.

to the tetracycline antibiotics matrix solution, which were formulated from the maximum concentration of surface water quality in Beijing [26]. As shown in **Fig. S5**, inorganic anions exerted slight effect on the adsorption of TCs over vivianite, but had little effect on the degradation of TCs. To further investigate whether the vivianite/TCs/PDS/UVL system can work well in the actual wastewater, the TCs degradation was conducted toward the simulated wastewater formulated from both tap water and lake water [53,54]. As illustrated in Fig. 5**a – 5c**, vivianite/TCs/PDS/UVL system displayed the outstanding activity in natural water and tap water, and the TCs-CTC (CTC in the TCs matrix) degradation efficiencies in lake water (100%) and tap water (100%) were higher than that in ultrapure water (90%) within 1 min. From the discussion above, it can be concluded that the vivianite/TCs/PDS/UVL system is very feasible for practical water remediation.

3.2.2.2. Effect of TCs degradation under visible light and real solar light irradiation. The optical absorption edge of vivianite is about 442 nm with E_g as ca 2.8 eV, indicating that vivianite could be excited by the visible light as well. From that point, a series of studies were conducted under LED visible light (VL) in this work. As depicted in Fig. 6**a and 6d**, no matter the concentration of TTC/OTC/CTC is 10.0 mg/L or 1.0 mg/L, the degradation efficiency of the vivianite/PDS/VL system can reach 100% within 10 min. The degradation efficiency of CTC in TCs antibiotics matrix with the concentration of 10.0 mg/L can only reach 90% in 10 min, while the TTC and OTC in tetracycline antibiotics matrix can be degraded to 100% within 10 min, further indicating that vivianite exhibited excellent catalytic activity for the tetracycline antibiotics decomposition under LED visible light. Considering that vivianite could accomplish outstanding photoactivated SR-AOP performances under LED UV and visible light, it might accomplish the identically photoactivation of PDS under real solar light (SL). As shown in Fig. 6**b and 6e**, it was worth noting that the TCs (10.0 mg/L and 1.0 mg/L) degradation efficiencies in the vivianite/PDS/SL system (100% within 1 or 2 min) were better than those under visible light (90% TCs-CTC degradation within 10 min), which could be attributed to the wide spectrum and high temperature under sunlight. The excellent catalytic performance in the vivianite/PDS/SL system could prove that the vivianite catalyst has promising application in real solar light for the goal of energy conservation. In addition, the TOC removal efficiencies were investigated under the different system (Fig. 6**c and 6f**). It can be seen clearly that ca. 80%, 78% and 40%~58% of TOC removal efficiencies were achieved in the UVL, VL and SL system within 30 min, respectively (Fig. 6**c**). However, the TOC removal efficiency decrease at higher TCs concentrations (Fig. 6**f**). And the order of TOC removal efficiencies was vivianite/PDS/UVL **>** vivianite/PDS/VL **>** vivianite/PDS/SL regardless of the pollutant concentration of 10.0 mg/L or 1.0 mg/L, which could be attributed to the higher energy of UV light [55].

3.3. Possible photoactivated SR-AOP mechanism over vivianite

The trapping experiments and ESR tests were carried out to further confirm the reactive oxygen species in the vivianite/PDS/UVL system. Herein, tertbutyl alcohol (TBA) is generally employed as scavenger of •OH radical, and methanol (MeOH) is scavenger for both $•SO_4^-$ and •OH [56,57]. Also, KI, benzoquinone (BQ) and L-histidine as scavengers to seize the h^+, $•O_2^-$ and nonradical singlet oxygen ($^1O_2$) [58]. In Fig. 7**a – 7c**, the TTC/OTC/CTC degradation efficiencies decreased in the presence of MeOH, TBA, KI and BQ, demonstrating that $•SO_4^-$, •OH, h^+, and $•O_2^-$ were involved in the vivianite/PDS/UVL system for TCs degradation. However, the catalytic degradation efficiencies of vivianite on TTC/OTC/CTC remained almost unchanged when L-histidine was added to the system, demonstrating that $^1O_2$ was not involved in the SR-AOP degradation toward TCs over vivianite. Similar results can be obtained by ESR spectra (**Fig. S6**), in which there were no TEMP-$^1O_2$ signals in the degradation process. The $•O_2^-$ can be detected in the vivianite/light system (Fig. 7**e**), which can be yielded as the CB value of vivianite being −0.62 eV *vs.* NHE, much more negative than the $O_2/•O_2^-$ potential (-0.33 eV *vs.* NHE). However, the weak peak of DMPO-$•O_2^-$ may be ascribed to the rapid recombination of photo-induced h^+ and e^-. For PDS without vivianite as catalyst upon the irradiation of UV light, the characteristic peaks of DMPO-$•SO_4^-$, DMPO-•OH and DMPO-$•O_2^-$ could be tested (Fig. 7**d and 7e**), demonstrating that PDS could be activated by UV light to generate $•SO_4^-$, •OH and $•O_2^-$ in the aqueous solution. And hydroperoxyl radical ($•HO_2$) generated by the protonation of $•O_2^-$ also can be found in ESR spectrum (Fig. 7**e**). PDS could be activated by the vivianite in the dark to produce the $•SO_4^-$, •OH, $•O_2^-$ and $•HO_2$, but the signals became more pronounced with the UV light irradiation, suggested that the synergetic effect of vivianite, UVL and PDS. These results confirmed the successful activation PDS by UVL to produce $•SO_4^-$, •OH, $•O_2^-$ and $•HO_2$, which then collectively contribute to the TCs degradation. As well, the generation of $•SO_4^-$ dosage has been quantified in vivianite/PDS/UVL and PDS/UVL (blank) systems. As shown in Fig. 7**f**, the concentration of $•SO_4^-$ produced in vivianite/PDS/UVL systems was 3.6 μM within 10 min, which was higher than the PDS/UVL systems (2.4 μM).

The outstanding performance of photoactivated SR-AOP over vivianite was explored by EIS techniques. The Nyquist arc radius of vivianite/UVL was smaller than vivianite/dark system (Fig. 8**a**), as the UV light illumination could reduce the charge transfer resistance significantly. The addition of PDS might reduce the charge transfer resistance of vivianite, implying that electron transfer was inclined to occur in photoactivated SR-AOP process.

As stated above, the parallel mechanisms of PDS activation by vivianite can be postulated as depicted in Fig. 8**c**. Firstly, upon the irradiation of UV light, vivianite can be excited to form photo-induced electrons and holes, in which the holes can directly oxide the organic pollutants. The $•O_2^-$ can be produced via the reaction between electrons and dissolved oxygen (Eqs. (4) and (5)) [26], which can also directly degrade TCs. Secondly, the photoelectrons activate persulfate subsequently to produce $•SO_4^-$ (Eq. (6)) [59], enhancing electron–hole separation efficiency to further boost the TCs degradation. Thirdly, one mole of PDS can produce two moles of radicals upon the irradiation of UV light with high energy (Eq. (7)) [59,60]. In addition, PDS could be

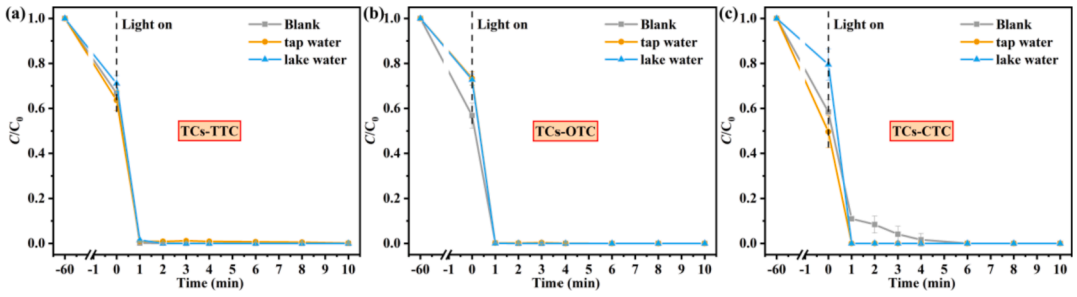

Fig. 5. The influence of different simulated wastewater on TCs removal efficiencies: (a) TCs-TTC, (b) TCs-OTC, (c) TCs-CTC. Reaction conditions: catalyst = 0.4 g/L, $[TCs\text{-}TTC, TCs\text{-}OTC, TCs\text{-}CTC]_0$ = 3.0 mg/L, solution volume = 50.0 mL, $[PDS]_0$ = 2.0 mM, unadjusted pH = 4.48.

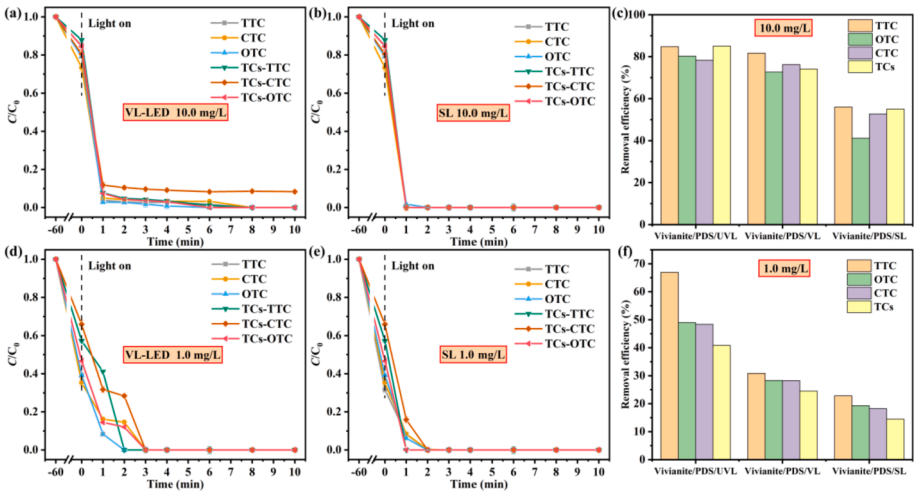

Fig. 6. Degradation of tetracycline antibiotics under different light conditions: (a, d) LED visible light, (b, e) real solar light; The TOC degradation of the tetracycline antibiotics within 30 min under different conditions: (c) 10.0 mg/L, (f) 1.0 mg/L.

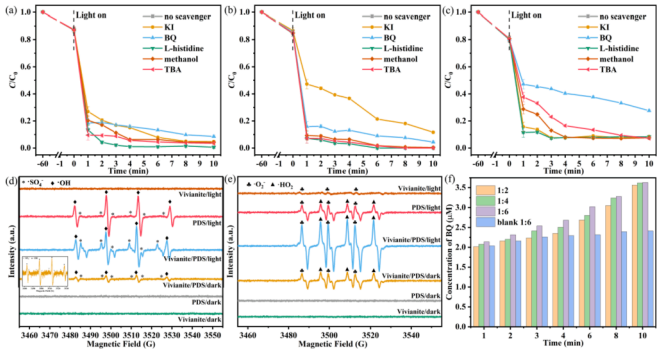

Fig. 7. Influences of different capturers on (a) TTC, (b) OTC, (c) CTC degradation activity with vivianite as catalyst. Reaction conditions: catalyst = 0.4 g/L, $[TTC, OTC, CTC]_0$ = 10.0 mg/L, solution volume = 50.0 mL, $[PDS]_0$ = 2.0 mM, unadjusted pH = 4.48, $[KI, BQ, L\text{-histidine}]_0$ = 5.0 mM, $[methanol, TBA]_0$ = 1000.0 mM. The ESR signals of (d) DMPO-$^{\bullet}SO_4^-$ and DMPO-$^{\bullet}OH$ (e) DMPO-$^{\bullet}O_2^-$ and DMPO-$^{\bullet}HO_2$ under different conditions; (f) The formed $^{\bullet}SO_4^-$ contents at different PDS:HBA ratios in vivianite/PDS/UVL system.

activated by vivianite catalyst, in which the Fe(II) specie might break the O-O bonds of $S_2O_8^{2-}$ anions to yield $^{\bullet}SO_4^-$ radicals (Eq. (8)) [59]. The presence of Fe^{2+} from the XPS test of the used vivianite echoed the above-stated analysis and discussion (Fig. 8**b**). Finally, a series of reactions (Eqs. (9) – (12)) occurred to generate various reactive radicals like $^{\bullet}OH$, $^{\bullet}O_2^-$ and $^{\bullet}HO_2$ to degrade TCs [60–62]. These results confirm that vivianite has excellent degradation performance of TCs with the aid of both PDS and UV light.

$$\text{vivianite} + h\nu \rightarrow e^- + h^+ \quad (4)$$

$$O_2 + e^- \rightarrow {}^{\bullet}O_2^- \quad (5)$$

$$S_2O_8^{2-} + e^- \rightarrow {}^{\bullet}SO_4^- + SO_4^{2-} \quad (6)$$

$$S_2O_8^{2-} + h\nu \rightarrow 2{}^{\bullet}SO_4^- \quad (7)$$

$$S_2O_8^{2-} + Fe^{2+} \rightarrow {}^{\bullet}SO_4^- + Fe^{3+} + SO_4^{2-} \quad (8)$$

$$^{\bullet}SO_4^- + H_2O \rightarrow SO_4^{2-} + {}^{\bullet}OH + H^+ \quad (9)$$

$$S_2O_8^{2-} + 2H_2O \rightarrow HO_2^- + 2SO_4^{2-} + 3H^+ \quad (10)$$

$$HO_2^- + S_2O_8^{2-} \rightarrow {}^{\bullet}SO_4^- + SO_4^{2-} + H^+ + {}^{\bullet}O_2^- \quad (11)$$

$$^{\bullet}O_2^- + H^+ \rightarrow {}^{\bullet}HO_2 \quad (12)$$

3.4. Possible degradation pathways and toxicity assessment

Intermediate products during the TCs degradation over vivianite were detected by HPLC–MS. In this work, possible degradation pathways of different TCs like TTC, OTC and CTC are discussed in the Supplementary Materials and shown in **Fig. S7**, **Fig. S8** and **Fig. S9**, respectively. The acute toxicity, developmental toxicity and bioaccumulation factor of TCs and their degradation intermediates were assessed by Toxicity Estimation Software (T.E.S.T.) based on quantitative structure–activity relationship (QSAR) prediction, which can be found in the Supplementary Materials and shown in **Fig. S10**.

The growth inhibition effects of *Escherichia coli* (*E. coli*) were used to test the toxicities of TCs and their intermediates [29]. As displayed in Fig. 9, the diameters of inhibition zones for TTC, OTC, CTC and TCs against *E. coli.* were 13.56 mm, 13.6 mm, 14.76 mm and 12.42 mm, respectively. The inhibition of TTC, OTC, CTC, TCs and their by-products against *E. coli.* decreased significantly within 10 min, and the diameters of inhibition zones were 7.83 mm, 8.52 mm, 8.57 mm and 8.13 mm respectively. Meanwhile, the removal efficiencies of TOC of TTC, OTC, CTC and TCs were 41.2%, 30.3%, 33.2% and 37.3% within 10 min, respectively. Extending the photoactivated SR-AOP reaction up to 30 min, the degradation efficiencies of TOC of TTC, OTC, CTC and TCs increased to 84.8%, 80.2%, 78.3% and 85.1%. It was worth noting that the diameters of the inhibition zones were almost consistent with the blank experiment without TCs within 30 min, demonstrated that the transformation products of TCs via photoactivated SR-AOP over vivianite did not maintain their inhibitory effect towards *E. coli.* These results demonstrated that the degradation of TCs over vivianite may resulted in decreasing toxicity toward *E. coli.*

3.5. Reusability and stability of vivianite

Both the stability and reusability are essential to the future practical application. Fig. 10**a – 10d** presented the vivianite maintained a stable efficiency for TTC, OTC, CTC and TCs degradation over five reuse cycles. And the degradation performances of TTC, OTC, CTC and TCs in vivianite/PDS/UVL system remained at 100% without a significant decrement after five runs' use, demonstrated the remarkable reusability of vivianite. Additionally, any alterations can't be observed in morphologies, phase and composition of the used vivianite based on the PXRD and SEM results (Fig. 10**e and 10f**), confirming the good stability of vivianite. In addition, the leaching of Fe was investigated by ICP-OES

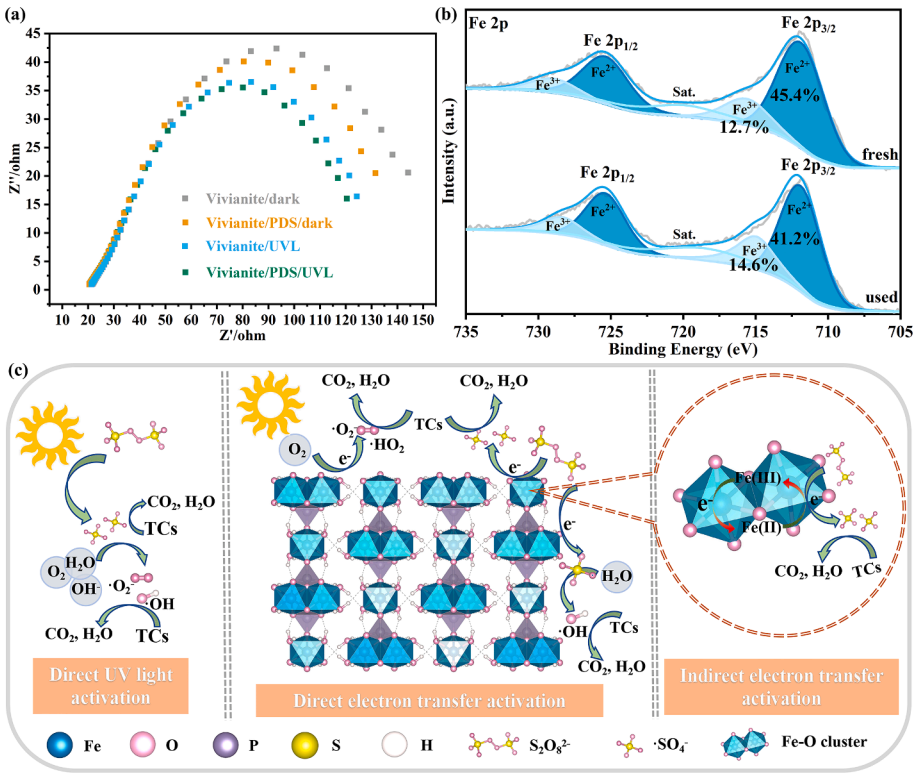

Fig. 8. (a) Electrochemical impedance spectroscopy of various oxidation processes; (b) Fe 2p XPS of the used vivianite; (c) Illustration of possible mechanism of photoactivated SR-AOP oxidation of TCs over vivianite under LED UV light.

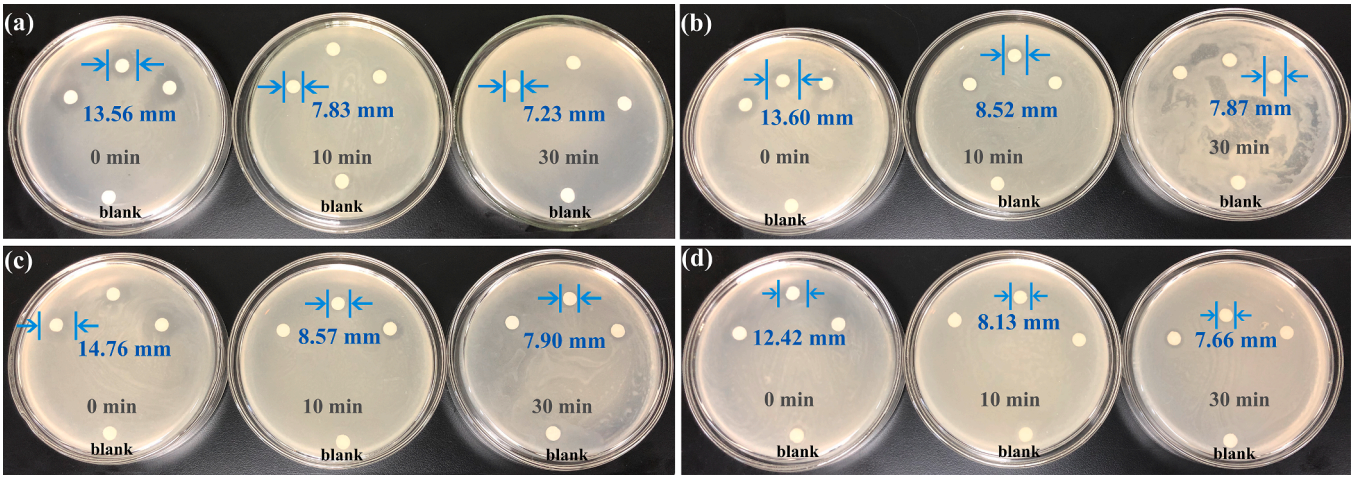

Fig. 9. Images and diameters of inhibition zones of (a) TTC, (b) OTC, (c) CTC, (d) TCs and its degradation intermediates against *E. coli* over Vivianite/PDS/UVL system.

after five cycles (Fig. S11), and the concentrations of leached Fe were conformed to the discharge standard of iron ions [63].

3.6. Universality of vivianite as AOPs catalyst

Fig. S12**a** revealed that the degradation of fluoroquinolone antibacterial (norfloxacin (NOR), enrofloxacin (ENR) and ciprofloxacin (CIP)), estrogenic hormone (estradiol (17β-E2)), antiviral drug (chloroquine (CQ)), and pesticide (2,4-Dichlorophenoxyacetic acid (2,4-D) and atrazine (ATZ)) by vivianite activated PDS under UV light irradiation, indicating that vivianite could effectively remove different kinds of pollutants. In addition, vivianite also could photoactivated PMS and H_2O_2 to degrade TCs completely within 10 min (Fig. S12**b and S12c**), indicating its wide universality. Consequently, it was considered that vivianite might display great application potential in the field of advanced oxidation process.

3.7. The photoactivated SR-AOP performance of vivianite recovered from WWTP

In order to explore the advanced oxidation activity of real vivianite recovered from WWTP, we synthesized the real vivianite mineral from sewage as the previously reports [64]. As shown in Fig. S13**a**, the real vivianite mineral could remove ca. 50% of TTC, OTC and CTC in the dark. And the TTC, OTC and CTC could be degraded completely within 10 min in the presence of both recovered vivianite and PDS under the

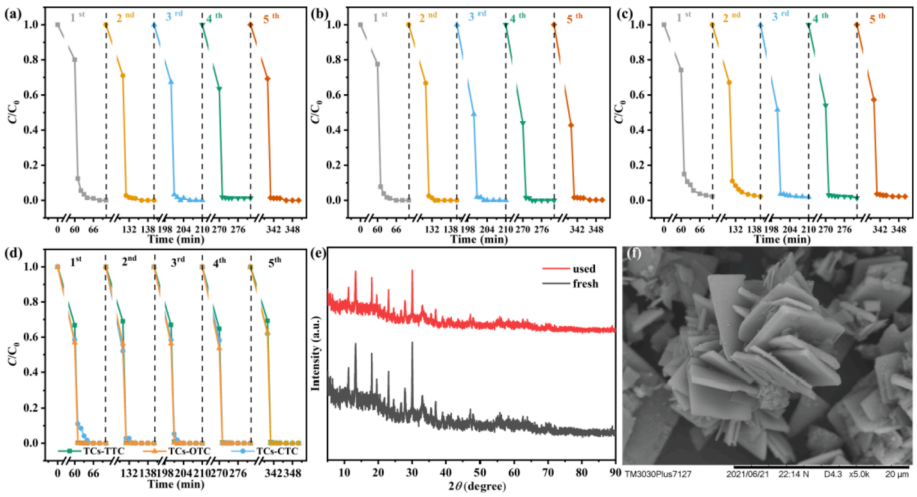

Fig. 10. Recycling runs in the degradation of (a) TTC, (b) OTC, (c) CTC, (d) TCs in Vivianite/PDS/UVL system. Reaction conditions: catalyst = 0.4 g/L, [TTC, OTC, CTC]$_0$ = 10.0 mg/L, [TCs-TTC, TCs-OTC, TCs-CTC]$_0$ = 3.0 mg/L, solution volume = 50.0 mL, [PDS]$_0$ = 2.0 mM, unadjusted pH = 4.48. (e) PXRD and (f) SEM of vivianite after the cyclic experiment.

LED UV light, LED visible light and real solar light irradiation. Similarly, the real vivianite mineral could activate PDS effectively for the complete elimination toward the matrix of TTC, OTC and CTC (**Fig. S13b**). Consequently, we demonstrated that the real vivianite mineral recovered from WWTP could be the AOP catalyst for effective elimination toward different organic pollutants.

4. Conclusions

This study demonstrated that the vivianite as an effective heterogeneous catalyst could activate persulfate to degrade tetracycline antibiotics completely under LED UV, visible and real solar light irradiation within 10 min. Mechanism study revealed that vivianite successfully activation PDS by UVL to produce various oxidative radicals ((like $^{\bullet}SO_4^-$, $^{\bullet}OH$, $^{\bullet}O_2^-$ and $^{\bullet}HO_2$), which then collectively contribute to the TCs degradation. The superior performance of PDS activation over vivianite under LED UV light irradiation can not only oxidize TCs but also lead to high TOC removal efficiency and low acute toxicity. Moreover, vivianite displayed satisfactory stability, which was affirmed by the low leaching iron ion during the cyclic tests. In future, more efforts will be put to achieve real environmental remediation applications of vivianite harvested from the wastewater treatment process.

Declaration of Competing Interest

The authors declare that they have no known competing financial interests or personal relationships that could have appeared to influence the work reported in this paper.

Data availability

Data will be made available on request.

Acknowledgements

This work was supported by National Natural Science Foundation of China (22176012, 51878023), Beijing Natural Science Foundation (8202016), National Key Research and Development Program of China (2016YFC0402505), Beijing Talent Project (2020A27), Science and Technology General Project of Beijing Municipal Education Commission (KM202110016010), The Fundamental Research Funds for Beijing University of Civil Engineering and Architecture (X20147/X20141/X20135/X20146) and BUCEA Doctor Graduate Scientific Research Ability Improvement Project (DG2021004).

Appendix A. Supplementary data

Supplementary data to this article can be found online at https://doi.org/10.1016/j.cej.2022.137784.

References

[1] X. Hao, C. Wang, M.C.M. van Loosdrecht, Y. Hu, Looking beyond struvite for P-recovery, Environ. Sci. Technol. 47 (2013) 4965–4966, https://doi.org/10.1021/es401140s.
[2] S. Wang, J. An, Y. Wan, Q. Du, X. Wang, X. Cheng, N. Li, Phosphorus competition in bioinduced vivianite recovery from wastewater, Environ. Sci. Technol. 52 (2018) 13863–13870, https://doi.org/10.1021/acs.est.8b03022.
[3] C. Zhang, A. Guisasola, J.A. Baeza, A review on the integration of mainstream P-recovery strategies with enhanced biological phosphorus removal, Water Res. 212 (2022), 118102, https://doi.org/10.1016/j.watres.2022.118102.
[4] Q. Wang, T.-H. Kim, K. Reitzel, N. Almind-Jørgensen, U.G. Nielsen, Quantitative determination of vivianite in sewage sludge by a phosphate extraction protocol validated by PXRD, SEM-EDS, and ^{31}P NMR spectroscopy towards efficient vivianite recovery, Water Res. 202 (2021), 117411, https://doi.org/10.1016/j.watres.2021.117411.
[5] P. Wilfert, A.I. Dugulan, K. Goubitz, L. Korving, G.J. Witkamp, M.C.M. Van Loosdrecht, Vivianite as the main phosphate mineral in digested sewage sludge and its role for phosphate recovery, Water Res. 144 (2018) 312–321, https://doi.org/10.1016/j.watres.2018.07.020.
[6] R. Liu, D. Zhao, In situ immobilization of Cu(II) in soils using a new class of iron phosphate nanoparticles, Chemosphere 68 (2007) 1867–1876, https://doi.org/10.1016/j.chemosphere.2007.03.010.
[7] K. Taylor, K. Hudson-Edwards, A.J. Bennett, V. Vishnyakov, Early diagenetic vivianite [$Fe_3(PO_4)_2 \cdot 8H_2O$] in a contaminated freshwater sediment and insights into zinc uptake: a mu-EXAFS, mu-XANES and Raman study, Appl. Geochem. 23 (2008), https://doi.org/10.1016/j.apgeochem.2008.01.009.
[8] V. Thinnappan, C.M. Merrifield, F.S. Islam, D.A. Polya, P. Wincott, R.A. Wogelius, A combined experimental study of vivianite and As(V) reactivity in the pH range 2–11, Appl. Geochem. 23 (2008) 3187–3204, https://doi.org/10.1016/j.apgeochem.2008.07.001.
[9] E.M. Muehe, G. Morin, L. Scheer, P.L. Pape, I. Esteve, B. Daus, A. Kappler, Arsenic (V) incorporation in vivianite during microbial reduction of Arsenic(V)-bearing biogenic Fe(III) (oxyhydr)oxides, Environ. Sci. Technol. 50 (2016) 2281–2291, https://doi.org/10.1021/acs.est.5b04625.
[10] H. Veeramani, D.S. Alessi, E.I. Suvorova, J.S. Lezama-Pacheco, J.E. Stubbs, J. O. Sharp, U. Dippon, A. Kappler, J.R. Bargar, R. Bernier-Latmani, Products of abiotic U(VI) reduction by biogenic magnetite and vivianite, Geochim. Cosmochim. Ac. 75 (2011) 2512–2528, https://doi.org/10.1016/j.gca.2011.02.024.
[11] S. Bae, Y. Sihn, D. Kyung, S. Yoon, T. Eom, U. Kaplan, H. Kim, T. Schäfer, S. Han, W. Lee, Molecular identification of Cr(VI) removal mechanism on vivianite surface, Environ. Sci. Technol. 52 (2018) 10647–10656, https://doi.org/10.1021/acs.est.8b01614.
[12] M.K. Ahmed, S.F. Mansour, R. Ramadan, M. Afifi, M.S. Mostafa, S.I. El-dek, V. Uskoković, Tuning the composition of new brushite/vivianite mixed systems for

superior heavy metal removal efficiency from contaminated waters, J. Water Process Eng. 34 (2020), 101090, https://doi.org/10.1016/j.jwpe.2019.101090.
[13] M. Etique, S. Bouchet, J.M. Byrne, L.K. ThomasArrigo, R. Kaegi, R. Kretzschmar, Mercury reduction by nanoparticulate vivianite, Environ. Sci. Technol. 55 (2021) 3399–3407, https://doi.org/10.1021/acs.est.0c05203.
[14] M.K. Ahmed, M. Afifi, S.F. Mansour, H.A. Ibrahium, S.A.A. Aldulmani, N. S. Awwad, Morphological behaviors of brushite/vivianite nanocomposites and their potency for Se(IV) and Cd(II) removal from aqueous solutions, Mater. Chem. Phys. 259 (2021), 124057, https://doi.org/10.1016/j.matchemphys.2020.124057.
[15] T. Prot, W. Pannekoek, C. Belloni, A.I. Dugulan, R. Hendrikx, L. Korving, M.C. M. van Loosdrecht, Efficient formation of vivianite without anaerobic digester: Study in excess activated sludge, J. Environ. Chem. Eng. 10 (2022), 107473, https://doi.org/10.1016/j.jece.2022.107473.
[16] R. Wang, P. Wilfert, I. Dugulan, K. Goubitz, L. Korving, G.-J. Witkamp, M.C.M. van Loosdrecht, Fe(III) reduction and vivianite formation in activated sludge, Sep. Purif. Technol. 220 (2019) 126–135, https://doi.org/10.1016/j.seppur.2019.03.024.
[17] P. Wilfert, A. Mandalidis, A.I. Dugulan, K. Goubitz, L. Korving, H. Temmink, G. J. Witkamp, M.C.M. Van Loosdrecht, Vivianite as an important iron phosphate precipitate in sewage treatment plants, Water Res. 104 (2016) 449–460, https://doi.org/10.1016/j.watres.2016.08.032.
[18] Y. Li, W. Xiang, T. Zhou, M. Huang, C. Wang, X. Wu, J. Mao, P. Wang, Visible light induced efficient activation of persulfate by a carbon quantum dots (CQDs) modified γ-Fe_2O_3 catalyst, Chin. Chem. Lett. 31 (2020) 2757–2761, https://doi.org/10.1016/j.cclet.2020.01.032.
[19] X.-H. Yi, C.-C. Wang, Elimination of emerging organic contaminants in wastewater by advanced oxidation process over iron-based MOFs and their composites, Prog. in Chem. 33 (2021) 471–489, https://doi.org/10.7536/PC200562.
[20] R. Guo, B. Xi, C. Guo, X. Cheng, N. Lv, W. Liu, A.G.L. Borthwick, J. Xu, Persulfate-based advanced oxidation processes: The new hope brought by nanocatalyst immobilization, Environ. Function. Mater. (2022), https://doi.org/10.1016/j.efmat.2022.05.004.
[21] X. Du, M. Zhou, Strategies to enhance catalytic performance of metal–organic frameworks in sulfate radical-based advanced oxidation processes for organic pollutants removal, Chem. Eng. J. 403 (2021), 126346, https://doi.org/10.1016/j.cej.2020.126346.
[22] B. Kaur, L. Kuntus, P. Tikker, E. Kattel, M. Trapido, N. Dulova, Photo-induced oxidation of ceftriaxone by persulfate in the presence of iron oxides, Sci. Total Environ. 676 (2019) 165–175, https://doi.org/10.1016/j.scitotenv.2019.04.277.
[23] C. Kim, J.-Y. Ahn, T.Y. Kim, W.S. Shin, I. Hwang, Activation of persulfate by nanosized zero-valent iron (NZVI): mechanisms and transformation products of NZVI, Environ. Sci. Technol. 52 (2018) 3625–3633, https://doi.org/10.1021/acs.est.7b05847.
[24] G. Zhao, J. Zou, X. Chen, L. Liu, Y. Wang, S. Zhou, X. Long, J. Yu, F. Jiao, Iron-based catalysts for persulfate-based advanced oxidation process: Microstructure, property and tailoring, Chem. Eng. J. 421 (2021), 127845, https://doi.org/10.1016/j.cej.2020.127845.
[25] J.-S. Wang, X.-H. Yi, X. Xu, H. Ji, A.M. Alanazi, C.-C. Wang, C. Zhao, Y.V. Kaneti, P. Wang, W. Liu, Y. Yamauchi, Eliminating tetracycline antibiotics matrix via photoactivated sulfate radical-based advanced oxidation process over the immobilized MIL-88A: Batch and continuous experiments, Chem. Eng. J. 431 (2022), 133213, https://doi.org/10.1016/j.cej.2021.133213.
[26] X.-H. Yi, H. Ji, C.-C. Wang, Y. Li, Y.-H. Li, C. Zhao, A. Wang, H. Fu, P. Wang, X. Zhao, W. Liu, Photocatalysis-activated SR-AOP over PDINH/MIL-88A(Fe) composites for boosted chloroquine phosphate degradation: Performance, mechanism, pathway and DFT calculations, Appl. Catal. B: Environ. 293 (2021), 120229, https://doi.org/10.1016/j.apcatb.2021.120229.
[27] X.-W. Zhang, F. Wang, C.-C. Wang, P. Wang, H. Fu, C. Zhao, Photocatalysis activation of peroxodisulfate over the supported Fe_3O_4 catalyst derived from MIL-88A(Fe) for efficient tetracycline hydrochloride degradation, Chem. Eng. J. 426 (2021), 131927, https://doi.org/10.1016/j.cej.2021.131927.
[28] A. Mohammad, M.E. Khan, M.H. Cho, T. Yoon, Adsorption promoted visible-light-induced photocatalytic degradation of antibiotic tetracycline by tin oxide/cerium oxide nanocomposite, Appl. Surf. Sci. 565 (2021), 150337, https://doi.org/10.1016/j.apsusc.2021.150337.
[29] J. Li, L. Zhao, R. Zhang, H.H. Teng, L.P. Padhye, P. Sun, Transformation of tetracycline antibiotics with goethite: Mechanism, kinetic modeling and toxicity evaluation, Water Res. 199 (2021), 117196, https://doi.org/10.1016/j.watres.2021.117196.
[30] J. Wang, D. Zhi, H. Zhou, X. He, D. Zhang, Evaluating tetracycline degradation pathway and intermediate toxicity during the electrochemical oxidation over a Ti/Ti_4O_7 anode, Water Res. 137 (2018) 324–334, https://doi.org/10.1016/j.watres.2018.03.030.
[31] A. Mohammad, M.E. Khan, M.H. Cho, T. Yoon, Fabrication of binary SnO_2/TiO_2 nanocomposites under a sonication-assisted approach: Tuning of band-gap and water depollution applications under visible light irradiation, Ceram. Int. 47 (2021) 15073–15081, https://doi.org/10.1016/j.ceramint.2021.02.065.
[32] M.E. Khan, A. Mohammad, W. Ali, A.U. Khan, W. Hazmi, W. Zakri, T. Yoon, Excellent visible-light photocatalytic activity towards the degradation of tetracycline antibiotic and electrochemical sensing of hydrazine by SnO_2–CdS nanostructures, J. Clean. Prod. 349 (2022), 131249, https://doi.org/10.1016/j.jclepro.2022.131249.
[33] C. Zhao, Y. Li, H. Chu, X. Pan, L. Ling, P. Wang, H. Fu, C.-C. Wang, Z. Wang, Construction of direct Z-scheme Bi_5O_7I/UiO-66-NH_2 heterojunction photocatalysts for enhanced degradation of ciprofloxacin: Mechanism insight, pathway analysis and toxicity evaluation, J. Hazard. Mater. 419 (2021), 126466, https://doi.org/10.1016/j.jhazmat.2021.126466.
[34] J. Liu, X. Cheng, X. Qi, N. Li, J. Tian, B. Qiu, K. Xu, D. Qu, Recovery of phosphate from aqueous solutions via vivianite crystallization: Thermodynamics and influence of pH, Chem. Eng. J. 349 (2018) 37–46, https://doi.org/10.1016/j.cej.2018.05.064.
[35] Y. Wu, C. Wang, S. Wang, J. An, D. Liang, Q. Zhao, L. Tian, Y. Wu, X. Wang, N. Li, Graphite accelerate dissimilatory iron reduction and vivianite crystal enlargement, Water Res. 189 (2021), 116663, https://doi.org/10.1016/j.watres.2020.116663.
[36] Y. Wu, J. Luo, Q. Zhang, M. Aleem, F. Fang, Z. Xue, J. Cao, Potentials and challenges of phosphorus recovery as vivianite from wastewater: A review, Chemosphere 226 (2019) 246–258, https://doi.org/10.1016/j.chemosphere.2019.03.138.
[37] Z. Li, Y. Gong, D. Zhao, Z. Dang, Z. Lin, Simultaneous immobilization of multi-metals in a field contaminated acidic soil using carboxymethyl-cellulose-bridged nano-chlorapatite and calcium oxide, J. Hazard. Mater. 407 (2021), 124786, https://doi.org/10.1016/j.jhazmat.2020.124786.
[38] B. Zhang, L. Wang, Y. Li, Fractionation and identification of iron-phosphorus compounds in sewage sludge, Chemosphere 223 (2019) 250–256, https://doi.org/10.1016/j.chemosphere.2019.02.052.
[39] E. Walpersdorf, C.B. Koch, L. Heiberg, D.W. O'Connell, C. Kjaergaard, H.C. B. Hansen, Does vivianite control phosphate solubility in anoxic meadow soils? Geoderma 193–194 (2013) 189–199, https://doi.org/10.1016/j.geoderma.2012.10.003.
[40] X.-H. Yi, S.-Q. Ma, X.-D. Du, C. Zhao, H. Fu, P. Wang, C.-C. Wang, The facile fabrication of 2D/3D Z-scheme g-C_3N_4/UiO-66 heterojunction with enhanced photocatalytic Cr(VI) reduction performance under white light, Chem. Eng. J. 375 (2019), 121944, https://doi.org/10.1016/j.cej.2019.121944.
[41] J. Liu, X. Zhang, Q. Zhong, J. Li, H. Wu, B. Zhang, L. Jin, H.B. Tao, B. Liu, Electrostatic self-assembly of a AgI/$Bi_2Ga_4O_9$ p–n junction photocatalyst for boosting superoxide radical generation, J. Mate. Chem. A 8 (2020) 4083–4090, https://doi.org/10.1039/C9TA13724F.
[42] F. Wang, H. Fu, F.-X. Wang, X.-W. Zhang, P. Wang, C. Zhao, C.-C. Wang, Enhanced catalytic sulfamethoxazole degradation via peroxymonosulfate activation over amorphous CoSx@SiO_2 nanocages derived from ZIF-67, J. Hazard. Mater. 423 (2022), 126998, https://doi.org/10.1016/j.jhazmat.2021.126998.
[43] F.-X. Wang, C.-C. Wang, X. Du, Y. Li, F. Wang, P. Wang, Efficient removal of emerging organic contaminants via photo-Fenton process over micron-sized Fe-MOF sheet, Chem. Eng. J. 429 (2022), 132495, https://doi.org/10.1016/j.cej.2021.132495.
[44] T. Sadeghi Rad, A. Khataee, S. Arefi-Oskoui, S. Sadeghi Rad, Y. Orooji, E. Gengec, M. Kobya, Graphene-based ZnCr layered double hydroxide nanocomposites as bactericidal agents with high sonophotocatalytic performances for degradation of rifampicin, Chemosphere 286 (2022), 131740, https://doi.org/10.1016/j.chemosphere.2021.131740.
[45] J.-Q. Li, Z.-W. Zhou, X. Li, Y.-L. Yang, J.-F. Gao, R. Yu, H.-P. Wang, N. Wang, Synergistically boosting sulfamerazine degradation via activation of peroxydisulfate by photocatalysis of Bi_2O_3-TiO_2/PAC under visible light irradiation, Chem. Eng. J. 428 (2022), 132613, https://doi.org/10.1016/j.cej.2021.132613.
[46] Y. Zhang, J. Zhou, J. Chen, X. Feng, W. Cai, Rapid degradation of tetracycline hydrochloride by heterogeneous photocatalysis coupling persulfate oxidation with MIL-53(Fe) under visible light irradiation, J. Hazard. Mater. 392 (2020), 122315, https://doi.org/10.1016/j.jhazmat.2020.122315.
[47] C. Zhao, J. Wang, X. Chen, Z. Wang, H. Ji, L. Chen, W. Liu, C.-C. Wang, Bifunctional $Bi_{12}O_{17}Cl_2$/MIL-100(Fe) composites toward photocatalytic Cr(VI) sequestration and activation of persulfate for bisphenol A degradation, Sci. Total Environ. 752 (2021), 141901, https://doi.org/10.1016/j.scitotenv.2020.141901.
[48] C.-H. Han, H.-D. Park, S.-B. Kim, V. Yargeau, J.-W. Choi, S.-H. Lee, J.-A. Park, Oxidation of tetracycline and oxytetracycline for the photo-Fenton process: Their transformation products and toxicity assessment, Water Res. 172 (2020), 115514, https://doi.org/10.1016/j.watres.2020.115514.
[49] Y. Yue, C. Shen, Y. Ge, Biochar accelerates the removal of tetracyclines and their intermediates by altering soil properties, J. Hazard. Mater. 380 (2019), 120821, https://doi.org/10.1016/j.jhazmat.2019.120821.
[50] Q. Zhang, L. Jiang, J. Wang, Y. Zhu, Y. Pu, W. Dai, Photocatalytic degradation of tetracycline antibiotics using three-dimensional network structure perylene diimide supramolecular organic photocatalyst under visible-light irradiation, Appl. Catal. B: Environ. 277 (2020), 119122, https://doi.org/10.1016/j.apcatb.2020.119122.
[51] R. Guan, X. Yuan, Z. Wu, H. Wang, L. Jiang, J. Zhang, Y. Li, G. Zeng, D. Mo, Accelerated tetracycline degradation by persulfate activated with heterogeneous magnetic $Ni_xFe_{3-x}O_4$ catalysts, Chem. Eng. J. 350 (2018) 573–584, https://doi.org/10.1016/j.cej.2018.05.195.
[52] Y.-X. Li, X. Wang, C.-C. Wang, H. Fu, Y. Liu, P. Wang, C. Zhao, S-TiO_2/UiO-66-NH_2 composite for boosted photocatalytic Cr(VI) reduction and bisphenol A degradation under LED visible light, J. Hazard. Mater. 399 (2020), 123085, https://doi.org/10.1016/j.jhazmat.2020.123085.
[53] Y.-H. Li, X.-H. Yi, Y.-X. Li, C.-C. Wang, P. Wang, C. Zhao, W. Zheng, Robust Cr(VI) reduction over hydroxyl modified UiO-66 photocatalyst constructed from mixed ligands: Performances and mechanism insight with or without tartaric acid, Environ. Res. 201 (2021), 111596, https://doi.org/10.1016/j.envres.2021.111596.
[54] X. Wei, C.-C. Wang, Y. Li, P. Wang, Q. Wei, The Z-scheme NH_2-UiO-66/PTCDA composite for enhanced photocatalytic Cr(VI) reduction under low-power LED

visible light, Chemosphere 280 (2021), 130734, https://doi.org/10.1016/j.chemosphere.2021.130734.
[55] S. Wu, H. Hu, Y. Lin, J. Zhang, Y.H. Hu, Visible light photocatalytic degradation of tetracycline over TiO_2, Chem. Eng. J. 382 (2020), 122842, https://doi.org/10.1016/j.cej.2019.122842.
[56] R. Zhang, M. Chen, Z. Xiong, Y. Guo, B. Lai, Highly efficient degradation of emerging contaminants by magnetic CuO@Fe_xO_y derived from natural mackinawite (FeS) in the presence of peroxymonosulfate, Chin. Chem. Lett. 33 (2022) 948–952, https://doi.org/10.1016/j.cclet.2021.07.029.
[57] R. Guo, Y. Chen, B. Liu, Y. Han, J. Gou, X. Cheng, Catalytic degradation of lomefloxacin by photo-assisted persulfate activation on natural hematite: Performance and mechanism, Chin. Chem. Lett. (2021), https://doi.org/10.1016/j.cclet.2021.11.061.
[58] A. Du, H. Fu, P. Wang, C. Zhao, C.-C. Wang, Enhanced catalytic peroxymonosulfate activation for sulfonamide antibiotics degradation over the supported CoS_x-CuS_x derived from ZIF-L(Co) immobilized on copper foam, J. Hazard. Mater. 426 (2022), 128134, https://doi.org/10.1016/j.jhazmat.2021.128134.
[59] S. Giannakis, K.-Y.-A. Lin, F. Ghanbari, A review of the recent advances on the treatment of industrial wastewaters by sulfate radical-based advanced oxidation processes (SR-AOPs), Chem. Eng. J. 406 (2021), 127083, https://doi.org/10.1016/j.cej.2020.127083.
[60] J. Yang, M. Zhu, D.D. Dionysiou, What is the role of light in persulfate-based advanced oxidation for water treatment? Water Res. 189 (2021), 116627 https://doi.org/10.1016/j.watres.2020.116627.
[61] J. Wang, S. Wang, Activation of persulfate (PS) and peroxymonosulfate (PMS) and application for the degradation of emerging contaminants, Chem. Eng. J. 334 (2018) 1502–1517, https://doi.org/10.1016/j.cej.2017.11.059.
[62] I. Velo-Gala, A. Torres-Pinto, C.G. Silva, B. Ohtani, A.M.T. Silva, J.L. Faria, Graphitic carbon nitride photocatalysis: the hydroperoxyl radical role revealed by kinetic modelling, Catal, Sci. Technol. 11 (2021) 7712–7726, https://doi.org/10.1039/D1CY01657A.
[63] J.-W. Wang, F.-G. Qiu, P. Wang, C. Ge, C.-C. Wang, Boosted bisphenol A and Cr(VI) cleanup over Z-scheme WO_3/MIL-100(Fe) composites under visible light, J. Clean. Prod. 279 (2021), 123408, https://doi.org/10.1016/j.jclepro.2020.123408.
[64] X. Hao, J. Zhou, C.-C. Wang, Vivianite formed in anaerobic digestion of excess sludge: Verification and analysis, China Water & Wastewater 34 (2018) 7–13, https://doi.org/10.19853/j.zgjsps.1000-4602.2018.13.002.